Supporting Information for "Strain-tunable linear dichroism and second-harmonic generation response in $TaOX_2$ (X = F, Cl, Br) monolayers: A first-principles study"

Yi-min Ding,[†] Qiang Wang,[†] Min Jiang,[†] Xiao-dan Liu,[†] Anqi Huang,[*,‡] Qingfang Li,[*,¶] and Youyong Li[*,§]

[†]*Department of General Education, Wuxi University, Wuxi 214105, China*

[‡] *School of Physics, Sun Yat-Sen University, Guangzhou, China*

[¶]*Department of Applied Physics, Nanjing University of Information Science&Technology, Nanjing 210044, China*

[§]*Institute of Functional Nano&Soft Materials (FUNSOM), Jiangsu Key Laboratory for Carbon-Based Functional Materials&Devices, Soochow University, Suzhou, 215123, China*

E-mail: huanganq8@mail2.sysu.edu.cn; qingfangli@nuist.edu.cn; yyli@suda.edu.cn

Calculation method for in-plane linear dichroism (LD)

$$LD = \frac{\varepsilon_2(x) - \varepsilon_2(y)}{\varepsilon_2(x) + \varepsilon_2(y)} \tag{1}$$

Carrier mobility calculation

In 2D the carrier mobility is given by the expression,[1]

$$\mu_{2\mathrm{D}} = \frac{e\hbar^3 C_{2\mathrm{D}}}{k_{\mathrm{B}} T m_{\mathrm{e}}^* m_{\mathrm{d}} (E_1^i)^2} \tag{2}$$

where m_{e}^* is the effective mass in the transport direction and m_{d} is the average effective mass determined by $m_{\mathrm{d}} = \sqrt{m_{\mathrm{x}}^* m_{\mathrm{y}}^*}$. The term E_1 represents the deformation potential constant of the valence-band minimum for hole or conduction-band maximum for electron along the transport direction, defined by $E_1^i = \Delta V_i/(\Delta l/l_0)$. Here ΔV_i is the energy change of the ith band under proper cell compression and dilatation, l_0 is the lattice constant in the transport direction and Δl is the deformation of l_0. The elastic modulus $C_{2\mathrm{D}}$ of the longitudinal strain in the propagation directions (both x and y) of the longitudinal acoustic wave is derived from $(E - E_0)/S_0 = C(\Delta l/l_0)^2/2$, where E is the total energy and S_0 is the lattice volume at equilibrium for a 2D system. The temperature used for the mobility calculations was 300 K.

Details for Real-time approach to nonlinear optical properties

Nonlinear optical properties are obtained within the real-time (RT) approach developed by Attaccalite et.al.[2–4]In this approach the time-dependent Schrödinger equation is integrated to obtain the time-dependent valence states $|v_{m\mathbf{k}}\rangle$, shown as:

$$i\hbar \frac{\mathrm{d}}{\mathrm{d}t} |v_{m\mathbf{k}}\rangle = \left(H_{\mathbf{k}}^{\mathrm{sys}} + i\mathcal{E} \cdot \tilde{\partial}_{\mathbf{k}} \right) |v_{m\mathbf{k}}\rangle \tag{3}$$

Herein, $H_{\mathbf{k}}^{\mathrm{sys}}$ is the system Hamiltonian–which is discussed later; $\mathcal{E} \cdot \tilde{\partial}_{\mathbf{k}}$ describes the coupling with the external field in the dipole approximation. While the Born–vonarmar periodic

boundary conditions are imposed, the coupling takes the form of a $\mathbf{k}$-derivative operator $\tilde{\partial}_{\mathbf{k}}$. The tilde indicates that the operator is'gauge covariant' and guarantees that the solutions of eqn (1) are invariant under unitary rotations among occupied states at $\mathbf{k}$.

From $|v_{m\mathbf{k}}\rangle$, the time-dependent polarization of the system $P_{\parallel}$ along the lattice vector a is calculated as,

$$P_{\parallel} = -\frac{ef \quad |\mathbf{a}|}{2\pi\nu N_{\mathbf{k}_\perp}} \sum_{\mathbf{k}_\perp} \mathrm{Im}\ \log \prod_{\mathbf{k}_\perp}^{N_{\mathbf{k}_\parallel}-1} \det S\Big(\mathbf{k}, \mathbf{k}+\mathbf{q}_\parallel\Big) \tag{4}$$

where $S\Big(\mathbf{k}, \mathbf{k}+\mathbf{q}_\parallel\Big)$ is the overlap matrix between $|v_{n\mathbf{k}}\rangle$ and $|v_{m\mathbf{k}+\mathbf{q}_\parallel}\rangle$. Furthermore, ν is the unit cell volume, f is the spin degeneracy, $N_{\mathbf{k}_\perp}$ and $N_{\mathbf{k}_\parallel}$ are respectively the number of $\mathbf{k}$ points along and perpendicular to the polarization direction, and $\mathbf{q}_\parallel$=$2\pi/(N_{\mathbf{k}_\parallel}\mathbf{a})$. Finally, the second harmonic coefficient is extracted from the power series of the polarization in the laser field $\mathcal{E}, \mathbf{P} = \chi^{(1)}\mathcal{E} + \chi^{(2)}\mathcal{E}\mathcal{E} + \chi^{(3)}\mathcal{E}\mathcal{E}\mathcal{E} + \ldots$.

In eqn (1), the model Hamiltonian chosen for $H^{\mathrm{sys}}_{\mathbf{k}}$ determines the level of approximation in the description of correlation effects in the SHG spectra. In this work, two different models for the system Hamiltonian are adopted: (i) the independent-particle approximation (IPA) model and and (ii) the real-time GW + BSE model. In IPA, the system Hamiltonian is simply evaluated from the Kohn-Sham DFT Hamiltonian with G_0W_0 corrections,

$$H^{\mathrm{sys}}_{\mathbf{k}} = H^{\mathrm{DFT}}_{\mathbf{k}} + \sum_{n\mathbf{k}} \Delta_{n\mathbf{k}} |v^0_{n\mathbf{k}}\rangle\langle v^0_{n\mathbf{k}}| \tag{5}$$

where $\Delta_{n\mathbf{k}} = E^{\mathbf{G_0W_0}}_{n\mathbf{k}} - E^{\mathbf{DFT}}_{n\mathbf{k}}$. This model is named as IPA-G_0W_0 for simplicity in the main text. In RT-GW+BSE model,

$$H^{\mathrm{sys}}_{\mathbf{k}} = H^{\mathrm{DFT}}_{\mathbf{k}} + \sum_{n\mathbf{k}} \Delta_{n\mathbf{k}} |v^0_{n\mathbf{k}}\rangle\langle v^0_{n\mathbf{k}}| + V_h(\mathbf{r})[\Delta\rho] + \Sigma_{\mathrm{SEX}}[\Delta\gamma] \tag{6}$$

where $\Delta\rho \equiv \rho(\mathbf{r};t) - \rho(\mathbf{r};t=0)$ is the variation of the electronic density and $\Delta\gamma \equiv \gamma(\mathbf{r},\mathbf{r}';t) - \gamma(\mathbf{r},\mathbf{r}';t=0)$ is the variation of the density matrix induced by the external field $\mathcal{E}$. $V_h(\mathbf{r})[\Delta\rho]$ is the Hartree potential and is responsible for the local-field effects orig-

inating from system inhomogeneities. The last term $\Sigma_{\mathrm{SEX}}[\Delta\gamma]$, is the screened-exchange self-energy that accounts for the electron-hole interaction, and is given by the convolution between the screened interaction W and $\Delta\gamma$. In the linear response limit, the GW+BSE model reproduces the optical absorption calculated by solving the Bethe-Salpeter equation.[5] This model is named as RT-G_0W_0+BSE for simplicity in the main text.

For eqn.(1), it can be numerically solved for $|v_{n\mathbf{k}}\rangle$ using the following algorithm developed by Crank and Nicholson[6] for both Hermitian and non-Hermitian type Hamiltonians:

$$|v_{n\mathbf{k}}(t+\Delta t)\rangle = \frac{I - i(\Delta t/2)H^{\mathrm{sys}}_{\mathbf{k}}(t)}{I + i(\Delta t/2)H^{\mathrm{sys}}_{\mathbf{k}}(t)}|v_{nk}(t)\rangle, \tag{7}$$

in which I is the identity element. The operation is strictly unitary for any value of time-step Δt. It turns out that if the applied field is a Dirac δ-type, the Fourier transformed responses can be evaluated at all frequencies. In our simulations, we switch on the monochromatic field at $t = t_0$. This sudden switch excites the eigenfrequencies of the system introducing spurious contributions to the nonlinear response. An imaginary term is added into the Hamiltonian to simulate a finite dephasing,

$$\Gamma = -\frac{i}{\gamma_{\mathrm{deph}}}\sum_{l}\left\{|v_{\mathbf{k},l}\rangle\langle v_{\mathbf{k},l}| - |v^0_{\mathbf{k},l}\rangle\langle v^0_{\mathbf{k},l}|\right\}, \tag{8}$$

where $|v^0_{\mathbf{k},l}\rangle$ are the valence bands of the unperturbed system and γ_{deph} is the dephasing rate. Then we run the simulations for a time much larger than $1/\gamma_{\mathrm{deph}}$ and sample $\mathbf{P}$(t) close to the end of the simulation. Since γ_{deph} determines also the spectral broadening, we cannot choose it arbitrary small. The smaller the dephasing rate is , the longer the simulation is. As an empirical parameter, the dephasing time $1/\gamma_{\mathrm{deph}}$ is usually set as 6.6 fs, which corresponds to a spectral broadening of approximately 0.2 eV.[2–4,7]

Atomic structures of $TaOX_2$ (X= F, Cl, Br) in POSCAR format

$NbOF_2$

1.00000000000000

5.9589295282229271 0.0000000000000001 0.0000000000000000

0.0000000000000002 3.8562482713380097 0.0000000000000000

0.0000000000000015 0.0000000000000017 27.0550994873000015

Ta F O

2 4 2

Direct

0.7272166138750078 0.5065854657273899 0.5000000000000000

0.2727833861249992 0.5065854657273899 0.5000000000000000

0.0000000000000000 0.5064833837409241 0.4498436831611033

0.0000000000000000 0.5064833837409241 0.5501562868389013

0.5000000000000000 0.5064821016318977 0.4406933403510152

0.5000000000000000 0.5064821016318977 0.5593066596489846

0.7417864083289866 0.0064489998997628 0.5000000000000000

0.2582135916710064 0.0064489998997628 0.5000000000000000

$NbOCl_2$

1.00000000000000

6.6921271756453855 0.0000000000000001 0.0000000000000000

0.0000000000000002 3.8661596365884625 0.0000000000000000

0.0000000000000016 0.0000000000000017 27.0550994873000015

Ta Cl O

2 4 2

Direct

0.7188298749474966 0.5064427399649923 0.5000000000000000

0.2811701250525034 0.5064427399649923 0.5000000000000000

0.0000000000000000 0.5066805516785291 0.4374138333765113

0.0000000000000000 0.5066805516785291 0.5625861366234932

0.5000000000000000 0.5064925208409123 0.4273550798140172

0.5000000000000000 0.5064925208409123 0.5726449201859827

0.7299756231114535 0.0063841385155264 0.5000000000000000

0.2700243768885394 0.0063841385155264 0.5000000000000000

$NbOBr_2$

1.00000000000000

7.0136880660190224 0.0000000000000001 0.0000000000000000

0.0000000000000002 3.8728948864501733 0.0000000000000000

0.0000000000000017 0.0000000000000017 27.0550994873000015

Ta Br O

2 4 2

Direct

0.7135640477048887 0.5062887180025938 0.5000000000000000

0.2864359522951186 0.5062887180025938 0.5000000000000000

0.0000000000000000 0.5070013319942356 0.4338769794962093

0.0000000000000000 0.5070013319942356 0.5661229905037954

0.5000000000000000 0.5062123194983020 0.4214886079975039

0.5000000000000000 0.5062123194983020 0.5785113920024962

0.7228115917284773 0.0064975815048644 0.5000000000000000

0.2771884082715155 0.0064975815048644 0.5000000000000000

Table S 1: The calculated elastic constants of $TaOX_2$ (X= F, Cl, Br) in unit of GPa.

	$TaOF_2$	$TaOCl_2$	$TaOBr_2$
C_{11}	87.43	57.276	73.64
C_{12}	-11.21	0.889	1.58
C_{22}	319.47	253.774	254.37
C_{66}	14.71	16.633	17.57

Table S 2: The calculated carrier effective masses m^* (m_0), deformation potential E_1 (eV), in-plane stiffness C_{2D} (N/m), and mobility μ ($cm^2 \cdot V^{-1} \cdot s^{-1}$) for electron (e) and hole (h) along the x and y directions in monolayer $TaOX_2$ (X= F, Cl, Br) at 300 K.

Carrier		m_x^*	m_y^*	E_{1x}	E_{1y}	C_{2D_x}	C_{2D_y}	μ_x	μ_y
e	$TaOF_2$	4.81	0.45	7.50	3.77	78.64	306.03	0.42	68.9
	$TaOCl_2$	1.69	0.41	1.66	3.88	70.52	268.31	22.1	110.4
	$TaOBr_2$	1.15	0.45	0.74	3.79	70.00	263.06	2458	898
h	$TaOF_2$	-12.27	-8.62	1.98	1.30	78.64	306.03	0.34	4.3
	$TaOCl_2$	-9.54	-7.57	1.30	0.39	70.52	268.31	1.63	57.8
	$TaOBr_2$	-8.66	-4.69	3.37	0.88	70.00	263.06	23.8	24.4

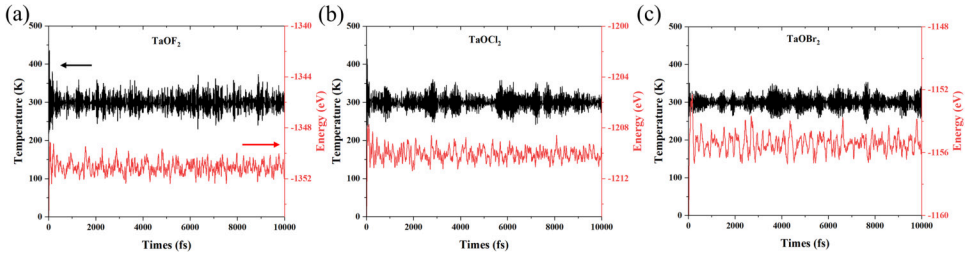

Figure S 1: Energy and temperature variations at 300 K from AIMD simulations within 4×5×1 supercell for $TaOX_2$ monolayers.

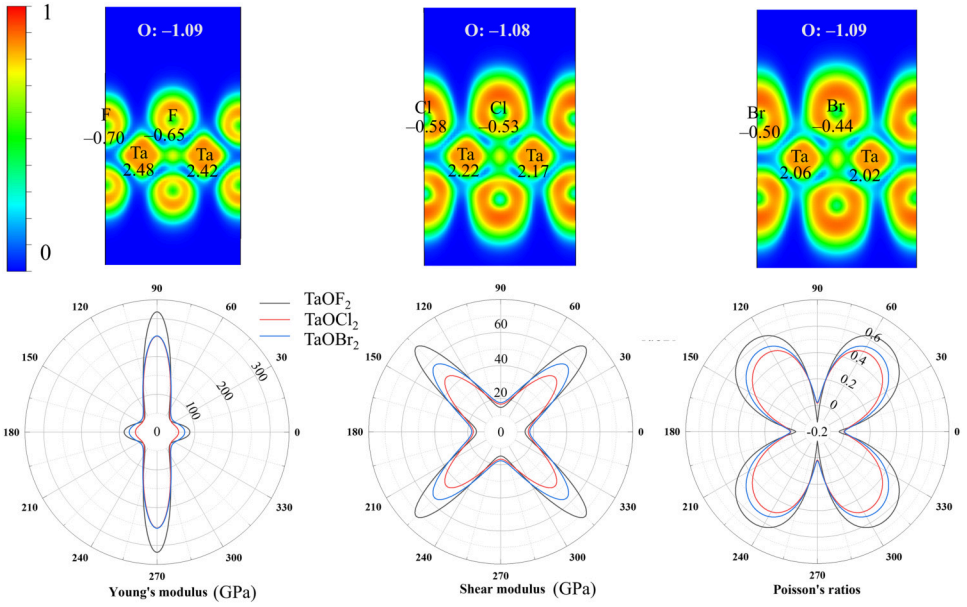

Figure S 2: Plot of electron localization function (ELF), Young's modulus, Shear modulus in unit of GPa and Poisson's ratio of $TaOX_2$ monolayers.

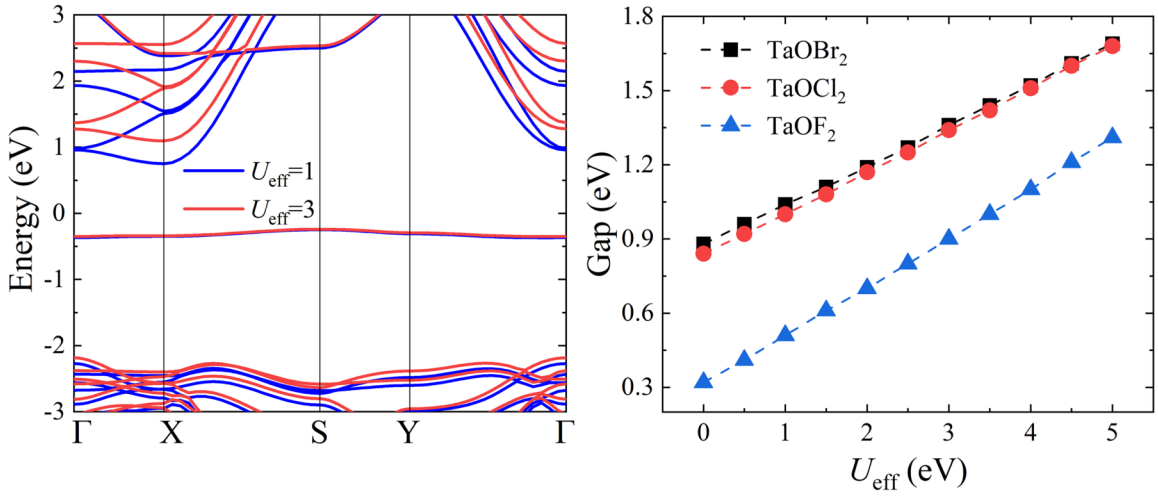

Figure S 3: Calculated band structures of $TaOCl_2$ from GGA+U method with different values of U_{eff} and U_{eff}-dependent variations of band gap for $TaOX_2$ monolayers.

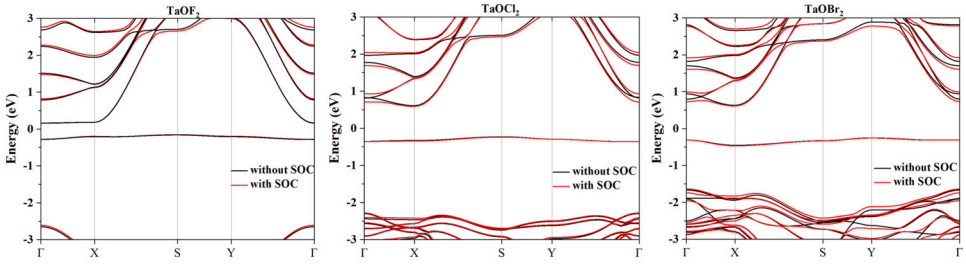

Figure S 4: Band structures with and without spin-orbit interactions for $TaOX_2$.

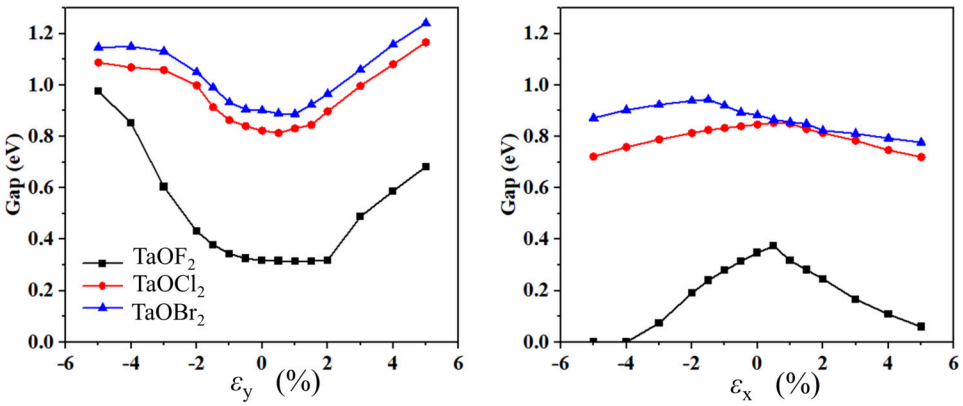

Figure S 5: Strain-dependent variations of band gap under X and Y direction of $TaOX_2$.

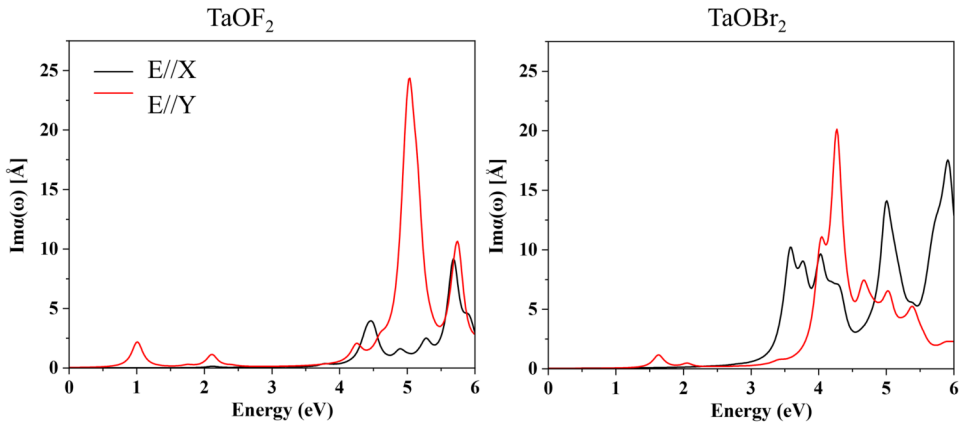

Figure S 6: Imaginary part of dielectric function of $TaOF_2$ and $TaOBr_2$.

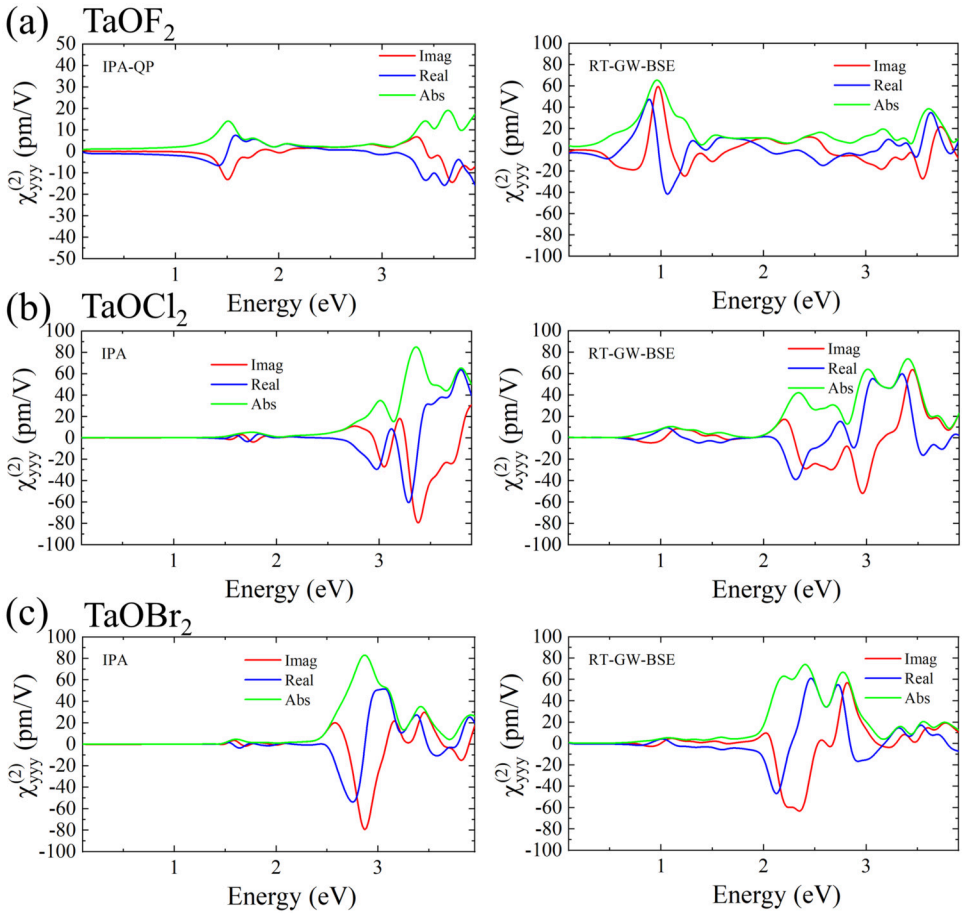

Figure S 7: Calculated SHG components $\chi^{(2)}_{yyy}$ at RT-IPA and RT-G_0W_0+BSE of $TaOX_2$.

References

(1) Qiao, J.; Kong, X.; Hu, Z.-X.; Yang, F.; Ji, W. High-mobility transport anisotropy and linear dichroism in few-layer black phosphorus. *Nature communications* **2014**, *5*, 4475.

(2) Attaccalite, C.; Grüning, M. Nonlinear Optics from an *Ab Initio* Approach by Means of the Dynamical Berry Phase: Application to Second- and Third-Harmonic Generation in Semiconductors. *Physical Review B* **2013**, *88*, 235113.

(3) Grüning, M.; Attaccalite, C. Second Harmonic Generation in h-BN and MoS 2 Monolayers: Role of Electron-Hole Interaction. *Physical Review B* **2014**, *89*, 081102.

(4) Attaccalite, C.; Nguer, A.; Cannuccia, E.; Grüning, M. Strong Second Harmonic Generation in SiC, ZnO, GaN Two-Dimensional Hexagonal Crystals from First-Principles Many-Body Calculations. *Physical Chemistry Chemical Physics* **2015**, *17*, 9533–9540.

(5) Attaccalite, C.; Grüning, M.; Marini, A. Real-time approach to the optical properties of solids and nanostructures: Time-dependent Bethe-Salpeter equation. *Physical Review B* **2011**, *84*, 245110.

(6) Crank, J.; Nicolson, P. A practical method for numerical evaluation of solutions of partial differential equations of the heat-conduction type. Mathematical Proceedings of the Cambridge Philosophical Society. 1947; pp 50–67.

(7) Mishra, H.; Bhattacharya, S. Exciton-Driven Giant Nonlinear Overtone Signals from Buckled Hexagonal Monolayer GaAs. *Physical Review B* **2020**, *101*, 155132.